Extreme Mechanics Letters 52 (2022) 101637

Contents lists available at ScienceDirect

Extreme Mechanics Letters

journal homepage: www.elsevier.com/locate/eml

Folding and deploying identical thick panels with spring-loaded hinges

Jingyi Yang, Yunlan Zhang, Manolis N. Chatzis, Zhong You *

Department of Engineering Science, University of Oxford, Parks Road, Oxford, OX1 3PJ, UK

ARTICLE INFO

Article history:
Received 30 September 2021
Received in revised form 22 December 2021
Accepted 17 January 2022
Available online 2 February 2022

Keywords:
Compact folding
Identical thick panels
Collision-free deployment
Spring-loaded hinges
Multiple DoFs

ABSTRACT

Many large deployable flat rigid arrays for aerospace applications, e.g., solar panels and reflectarray antennas, are preferably made from identical panels. It is challenging to pack them into a compact bundle before launching and deploy to a flat surface once in the orbit, especially if they are having bi-directional deployments. In this paper, we propose a folding scheme based on the Hamiltonian circuit that can successfully fold a chessboard-like array into a compact package with two stacks of panels without any voids. Since this approach leads to a multiple degrees-of-freedom (DoFs) assembly kinematically, simple spring-loaded hinges are used to synchronise the deployment. An effective optimisation method is subsequently proposed to select the stiffness of rotational joints to ensure a collision-free deployment. Dynamic simulation of the deployment and a collision detection method are incorporated into the optimisation process. By this approach, the trajectories of panels are sequenced to avoid collisions during the deployment, and the array always deploys to a flat surface from packaged stacks. Both the folding schemes and subsequent deployments were validated successfully by experiments. Though we consider only rectangular panels here, the approach can be extended to deployable arrays of any regular shape.

1. Introduction

Many large flat rigid surface structures exist in aerospace applications, e.g., solar panels and reflectarray antennas [1]. They are commonly made of many interlinked panels that folded to a small package before launching and subsequently deployed to a completely flat surface once reaching the orbit. The most widely used mechanism to fold rigid surface structures is zigzag folding, which expands and retracts unidirectionally [2]. Its simplicity and high packaging efficiency make it a preferred choice for many missions. If more panels are required, it is possible to just attach many stacks of solar panels to the main body of a satellite or a spacecraft [3,4]. However, these panels extend to form a long cantilever beam in the deployed state, making it rather flexible when the number of panels is high. Though this may not be a big issue for solar panels, surface inaccuracy due to flexibility makes it unsuitable for solar-array antennas. Other approaches also exist to overcome this problem. The bi-directional deployable surface structure based on the Miura-ori origami, which was utilised on an experiment flown on JAXA Space Flyer Unit, is an alternative [5]. Although it features a larger deployment ratio, large gaps have to be made between two successive panels because the Miura-ori cannot be applied to compactly fold panels of uniform thickness [6]. The winding mechanism is another bi-directional deployment mechanism, in which panels are wrapped around a polygonal hub [7–9]. It has the same drawback as the Miura-ori, and moreover, the width of the gaps between two consecutive panels increases as they go further away from the hub. In addition, panels at different locations are various in geometries. Other bi-directional folding methods have also been explored including origami-based thick panel folding schemes that eliminate the gaps between panels [10–12]. However, they commonly end up with either a non-flat surface in the fully deployed configuration or being unable to be packaged without any voids in the folded state.

In this paper, we explore the possibility of folding a rigid flat surface consisting of identical rigid panels with uniform thickness into the most compact stacks without any voids. Our problem is best illustrated with an example shown in Fig. 1. The left shows a chessboard-like array made from identical rigid rectangular panels connected by rotational joints. First, we want to find a systematic approach to design the rotational joints that connect the panels so that the array can be compactly packed into two stacks of fifteen panels each without any voids, as shown on the right, similar to the bi-directional folding schemes introduced earlier. Secondly, we want to devise a method to deploy the folded stacks to the flat surface.

We have discovered that the compact folding designs can be obtained by examining the Hamiltonian circuit for the chessboard-like array. It turns out that these designs generally lead to a system with multiple DoFs. Motorised rotational hinges can be

* Corresponding author.
E-mail address: zhong.you@eng.ox.ac.uk (Z. You).

https://doi.org/10.1016/j.eml.2022.101637

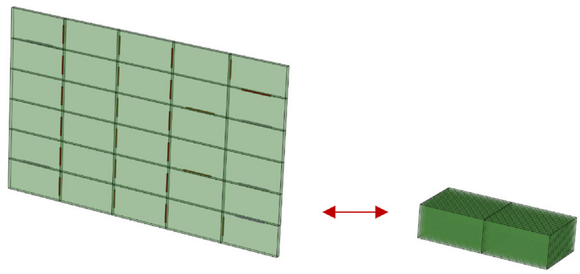

Fig. 1. An array consisting of identical rectangular panels in its fully deployed configuration (left) and compactly packaged configuration (right).

used to safely deploy panels from a compact configuration to a flat surface in a controlled manner, but the number of hinges, which is related to the number of DoF, can be high, which reduces the reliability. An alternative is to use spring-loaded hinges as rotational joints with their rest position coinciding with the fully deployable configuration of the array. The deployment is passively driven by releasing the elastic energy stored within the springs during folding. As the latter is a tried and tested method [13–15], it is adopted as a means of deployment. Since there is no control mechanism once the deployment starts, the stiffness of spring-loaded hinges must be chosen carefully to avoid any collision amongst panels during deployment. An optimisation process, including both dynamic modelling of the deployment process and collision detection, is carried out in our research to ensure this is the case. We also validated our designs by experiments.

The main content of this paper is structured as follows. A method to fold an array of identical rectangular panels into two compact stacks is introduced in Section 2. Section 3 contains the dynamic modelling of the deployment process and collision detection technique, based on which an optimisation method is set up. In Section 4, experiments on a prototype are presented to demonstrate the feasibility of our approach. The simulation results are benchmarked against the experimental results. Conclusions and discussions are presented in Section 5, which ends the paper.

2. Folding polygonal prisms into two compact stacks

In an array consisting of rectangular panels as shown in Fig. 2(a), each panel is adjacent to a minimum of two and a maximum of four neighbouring panels. Now consider an interior panel $P_{(2,\ 2)}$. When the array is folded into compact stacks, one of its neighbours, e.g., panel $P_{(2,\ 1)}$, may be folded over to the top of panel $P_{(2,\ 2)}$. Meanwhile, another neighbour, e.g., panel $P_{(3,\ 2)}$, may be folded over to the bottom of panel $P_{(2,\ 2)}$. Once both top and bottom surfaces of panel $P_{(2,\ 2)}$ are occupied by two of its neighbours, the other two, which are panels $P_{(1,\ 2)}$ and $P_{(2,\ 3)}$, can no longer be folded over because of no space left. Hence, only two panels can remain connected to panel $P_{(2,\ 2)}$ by rotational hinges. The same applies to exterior panels. Based on this principle, it becomes possible to design the location of rotational hinges using the Hamiltonian circuit [16]. It is a path that begins and ends on the same panel such that each panel is visited exactly once. A hinge is placed between a pair of panels if the Hamiltonian circuit crosses their common edge. Fig. 2(b) shows a Hamiltonian circuit for the 4 × 4 array.

Usually, more than one Hamiltonian circuit can be found within a given array. Finding all Hamiltonian circuits within an array consisting of a large number of rectangles is mathematically NP-complete, and the entire process takes time proportional to the number of panels, n [17]. For practical problems where n is finite, it is always feasible to find all Hamiltonian circuits.

Among the obtained Hamiltonian circuits for a given array, some of them cannot fulfil the two-stack packaging requirement. For instance, when the panels are clustered, they may not be divided into two stacks in parity. Hence, the Hamiltonian circuit approach provides a necessary but not sufficient condition for two-stack packaging. It is essential to examine all solutions obtained using the Hamiltonian circuits and check if they yield two-stack folded configurations. The validation can be achieved experimentally by making a card model. Based on our experience, a two-stacked foldable configuration can generally be obtained if a symmetrical Hamiltonian circuit is found in an array [18].

Feasible designs obtained by the Hamiltonian circuit often result in closed kinematic chains with multiple DoFs. For instance, the 4 × 4 array as shown in Fig. 2(b) is a closed kinematic chain of sixteen rigid panels connected by rotational joints, and its number of DoF is ten according to the Kutzbach criterion [19]. It is interesting to note that some of the rotational hinges, designed using the Hamiltonian circuit, may not be necessary. For instance, when folding the panels according to the design of Fig. 2(b), the pair of panels at the top centre, $P_{(1,\ 2)}$ and $P_{(1,\ 3)}$, will appear at the top of the stacks, whereas the pair of panels at the bottom centre, $P_{(2,\ 2)}$ and $P_{(2,\ 3)}$, end up at the bottom of the stacks. These panel pairs do not fold over each other. In other words, the rotational joints between these pairs need not be activated throughout the folding process. In fact, hinges and slits along the plane of symmetry of this array are also unnecessary. The eight panels on the middle two columns of the array can be merged to form four larger panels twice the size of the original ones, as shown in Fig. 2(c).

Merging some of the panels reduces the overall number of DoF. Moreover, the closed kinematic chain may become a combination of closed and open chains, as Fig. 2(c) shows. But still, the number of the DoFs for this spatial linkage is six using the Kutzbach criterion. Conventionally, at least six actuators are required to control the deployment of such a system. It is however possible to synchronise the motions of the panels using spring-loaded torsional hinges that are strain-free when the array is fully deployed. The stored energy amongst the hinges when the array is packaged drives its deployment passively as outlined in [13,14]. The deployment of the compactly packaged stacks is discussed next.

3. Deploying the stacks without collision

3.1. Dynamic model of the array deployment

The deployment of the array driven by releasing elastic energy stored in the hinges must be modelled using rigid body dynamics. A partially deployed loop consisting of n panels are shown in Fig. 3(a). A body-attached frame $\{i\}$ is fixed on panel i with its origin being the centroid of the panel and its axes x_i, y_i and z_i being oriented along the length, width and thickness direction of the panel, respectively. In the fully deployed configuration, z_i axes of all body-attached frames will point in the same direction. The hinges are placed along the edges of panels on either its top or bottom facet to facilitate compact folding. A generalised coordinate θ_i is introduced along each hinge h_i, allowing only the rotational DoF of the panel i with respect to its neighbour. Note that $0 \le \theta_i \le \pi$, with $\theta_i = 0$ and π represent fully deployed and fully folded configurations, respectively. During the deployment process, the position and orientation of the body-attached frame $\{i\}$ can be defined via the generalised coordinates. The topological graph of such an assembly with n panels and n hinges can be represented as a closed chain with an open chain attached, as

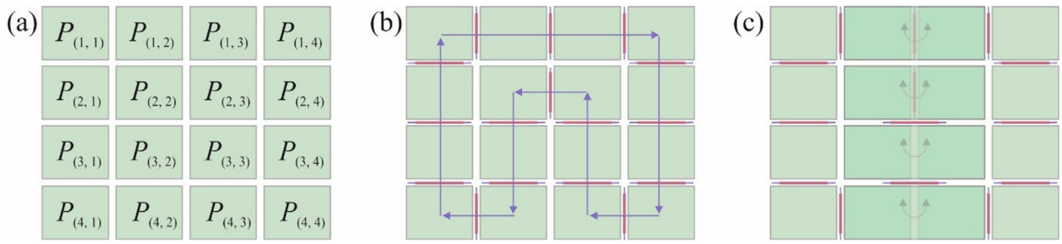

Fig. 2. (a) A4 × 4 array. (b) The Hamiltonian circuit of the array. Rotational hinges are placed on the edges where the circuit crosses from one panel to another. (c) Panels on the middle two columns of the array can be merged to form four larger panels that are twice the size of the original ones.

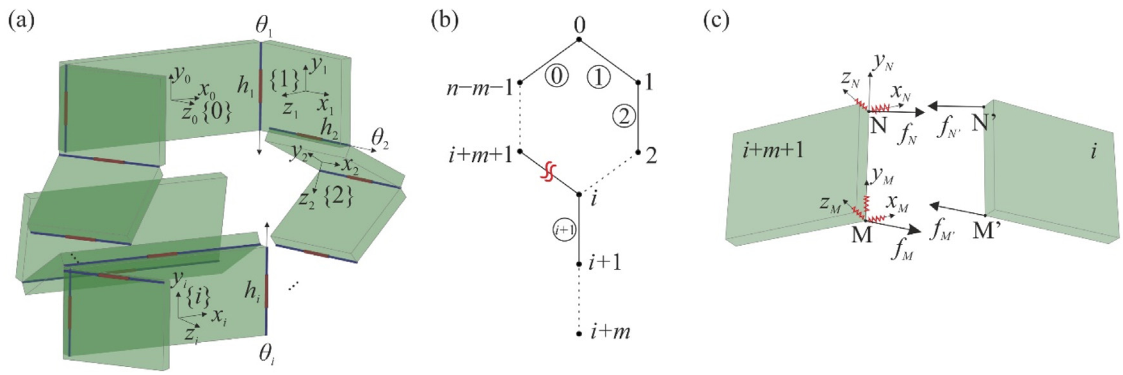

Fig. 3. (a) A generic configuration of panels that are connected by rotational hinges in red; (b) topological representation; (c) elements at the cut hinge (dampers are not shown). (For interpretation of the references to colour in this figure legend, the reader is referred to the web version of this article.)

shown in Fig. 3(b), where black dots represent panels and lines represent rotational hinges. The open chain has m rigid panels, which is the result when some panels are merged. The ground panel, which could be the one fixed to the main body of a satellite, is marked as panel 0.

When a closed chain exists in the system, the number of DoF is less than the number of hinges, indicating that the generalised coordinates that describe the configuration of the panels are no longer completely independent. The motion of panel i is not only a superposition of previous panels but also its next panels in the loop. One approach to compute the dynamics of such a system is through solving the equations of motion under some extra constraints brought together by the Lagrange multipliers, which would lead to a set of differential–algebraic equations (DAEs) [20]. However, solving DAEs would pose challenges computationally. The other way to tackle the dynamics of a closed chain is to replace some of the constraints with penalty springs [21], which is the method adopted here.

In our case, we superficially remove a hinge in the closed chain, turning the topological representation into two open branches as shown in Fig. 3(b) where the hinge between panels i and i+m+1 is removed. The removed hinge is referred to as the cut hinge hereafter. To make the open chains equivalent to the original one, translational springs with very high stiffness are placed at the cut hinge.

Now, all the generalised coordinates become independent because the current system corresponds to two open-loop chains originating from panel 0. The equations of motion (EOM) of the system can be written as a set of ordinary differential equations (ODEs) that can be integrated numerically in a more straightforward manner. For instance, the EOM of panel i can be obtained as

$$f_i = m_i a_i, \tag{1a}$$

$$\tau_i = I_i \alpha_i + \omega_i \times (I_i \omega_i) \tag{1b}$$

where f_i, m_i, and a_i denote the total force, the mass, and the linear acceleration of panel i, respectively, expressed in the body-attached frame $\{i\}$. τ_i, I_i, α_i, and ω_i are the total torque, the moment of inertia of the panel, the angular acceleration, and the angular velocity of panel i, respectively, with all the terms expressed in the body-attached frame $\{i\}$ [22,23].

Along each hinge h_i ($i = 0, 1, \ldots, n-1$), a torsional spring with constant stiffness k_i is placed to resist the angle of rotation θ_i. In the stowed configuration, each spring is pre-stressed with $\theta_i = \pi$, indicating a non-zero initial torque along each hinge. Within the permissible range of motion $0 \leq \theta_i \leq \pi$, the resultant torque can be written as

$$\tau_i = -k_i\theta_i + T_i(\omega) \tag{2}$$

where $T_i(\omega)$ is a torque resulting from viscous damping along h_i.

The energy loss along a hinge depends on many factors such as the spring chosen, how spring is connected to the panels, etc. It can be non-linear [24,25] if a clearance joint is used. However, in an elastic-hinge setup that was similar to that of this paper [15], it was verified that the viscous damping effect was a predominant source of energy dissipation. Thus, we conveniently assume that $T_i(\omega)$ is linearly proportional to and opposing the angular velocity ω_i.

$$T_i(\omega) = -c_i\omega_i \tag{3}$$

where c_i and ω_i are the damping coefficient and the angular velocity of the spring along hinge h_i.

The torsional spring and the damper contribute to modelling the toque along each hinge. When θ_i goes beyond the permissible range of motion, contact occurs between the side facets of the neighbouring panels i and $i-1$. To avoid penetration, the contact between the two side facets is modelled by a stiff torsional spring with spring stiffness k_s, which is much greater than k_i, and damping coefficient c_s. The overall torque τ_i is summarised as

$$\tau_i = \begin{cases} -k_s(\theta_i - \pi) - c_s\omega_i - c_i\omega_i & \text{if } \theta_i > \pi \\ -k_i\theta_i - c_i\omega_i & \text{if } 0 \leq \theta_i \leq \pi \\ -k_s\theta_i - c_s\omega_i - c_i\omega_i & \text{if } \theta_i < 0 \end{cases} \tag{4}$$

It is apparent that the contact spring and dampers k_s, c_s are only active when contact amongst panels i and $i-1$ occurs, i.e., $\theta_i > \pi$ or $\theta_i < 0$. More specifically, we set k_s to only allow penetrations of panels of no more than 0.1% of their length, while c_s is set based on material properties of the panels, shear modulus, and density in particular. When θ_i goes beyond the permissible range, the contact elements act in parallel with the torsional spring, which provides a nominal torque as elaborated in Eq. (4). However, while the contact is engaged within the aforementioned penetration range, it dominates the responses.

Let us now consider the applied force along the cut hinge, as demonstrated in Fig. 3(c), where MN and M′N′ denote the two edges of the cut hinge on the left and right rigid panels. A reference frame is originated at M, with x_{M}, y_{M} and z_{M} along the length, width and thickness direction of the panel, respectively. Another reference frame with the same orientation is set at point N. Five sets of virtual translational elastic springs with zero rest length and dampers are used to connect M with M′ and N with N′ along x_{M}, y_{M}, z_{M}, x_{N} and z_{N}, respectively. The stiffness of these virtual springs is sufficiently large so that once a small distance between M and M′, or N and N′, appears, there will be large restoring forces generated by the translational springs, bringing the distance back to zero. These forces can be calculated by

$$f_{\mathrm{M}} = -k_{\mathrm{M}} \Delta d_{\mathrm{MM'}} - c_{\mathrm{M}} \Delta \dot{d}_{\mathrm{MM'}} \tag{5}$$

where $\boldsymbol{\Delta} d_{\mathrm{MM'}}$ and $\boldsymbol{\Delta} \dot{d}_{\mathrm{MM'}}$ are the relative distance and the time rate of change of the relative distance between M with M′, k_{M} and c_{M} are spring stiffness and damping coefficient of the virtual translational spring that connects M with M′. The stiffness k_M is pre-defined to ensure that the separation between M with M′ is negligible in comparison to the motion-of-interest during the deployment process, yet the system is not too stiff to cause integration errors. A sufficient damping coefficient c_{M} is chosen so that the oscillations of the translational springs are attenuated. Likewise for points N with N′. As such, five DoFs are practically constrained along the axis of the cut hinge: three translational DoFs and two rotational DoFs, left with the only rotational DoF about MN. Along the active rotational DoF, a pre-stressed torsional spring and a damper with properties as described in Eq. (4) are modelled to rotate about y_{M} axis.

This system is implemented in Simscape, which uses a Newton formulation [26,27]. The time integration of the equation of motion is achieved via an explicit variable time-stepping Runge–Kutta (2, 3) pair [28]. A smaller increment in the time step is applied if the configuration is close to the singularity of the system. A Runge–Kutta (2,3) pair is chosen instead of Runge–Kutta (4, 5) pair for it is more computationally efficient at a given tolerance [29].

3.2. Collision detection

At this point, we should separate the "contacts" occurring when the values of θ_i across 0 or π, from all the other collisions. The former category of contact is not referred to as collision, and it is inevitable in this system. The latter is what we refer to as collisions, which is the focus of this section. Such collisions are more critical than the "contacts" because they can occur between the edges of a panel and any point on the surface of another panel leading to damages to the structure. It is important to point out that in this work, the dynamic model outlined earlier allows penetration amongst panels that are not connected by hinges. We use a collision detection method to detect when collisions take place and discard the dynamic modelling result after a collision is detected.

As rigid panels are convex polytopes, the configurations of any two panels can be represented by two sets U and W containing their corresponding coordinates of vertices. We then calculate the relative translations between the two convex polytopes. The set of translations that could cause interference of the two polytopes forms a new convex polytope, which is known as the Minkowski Difference (MD) of the two convex polytopes U and W [30,31]. MD is a binary operation that minuses all the points in W from those in U. The operation is detailed as follows.

$$U \oplus (-W) = \{u - w \,|u \in U, w \in W\} \tag{6}$$

If the two convex polytopes interfere, MD will contain the origin because one of the differences must be a zero vector if all points in W are subtracted from all points in U and they share a common coordinate. MD transforms the problem of intersection detection between two polytopes into determining if a point is within a new polytope or not. The geometrical collision detection can be conducted through GJK algorithm [30], which calculates MD of any given convex polytopes. It outputs proximal distance between the two panels, i.e. the minimal distance between them, if they do not interfere with each other. Otherwise, the proximal distance is set to zero.

The dynamic simulation contains a total of s time steps with the corresponding time instances being t_j ($j = 1, 2, \ldots$ s) evenly distributed from the start to the end of the deployment. By post-processing the dynamic simulation result, the positions of the panels are acquired. The algorithm outlined above enables us to obtain a vector, D_j, that contains all proximal distances between panel i ($i = 0, 1, \ldots, n-1$) and the other panels except the ones it shares a hinge with.

In ascending order of time instances, we examine every element in D_j. If one or more elements have zero value at t_J, the first collision takes place. The dynamic simulation result for subsequent time instances after t_J becomes invalid.

3.3. Collision avoidance via optimisation

In this multi-body system, the properties of the panels and their connectivity are pre-determined based on the applications. To avoid collisions in the deployment process, the trajectory of panels needs to be sequenced through carefully designing the hinge properties, including the stiffness and damping coefficient. On the other hand, the stiffness and damping coefficient to reflect the actual situation upon physical contact, k_s and c_s are pre-determined and hence, not to be optimised. We also give the hinge properties at the cut joint, including the virtual spring stiffness k_{M}, k_{N} and the damping coefficients c_{M}, c_{N}, which are set so that the separations between M and M′, N and N′ are negligible in comparison to the motion-of-interest during the deployment process while ensures the system being not too stiff to cause integration errors.

Therefore, the deciding parameters at a hinge that affect the trajectories of panels are the torsional spring stiffness k_i and the damping coefficient c_i. The stiffness of a spring can be tuned, but the damping of the elastic hinge is not easily tuned unless packing lubricants with different viscosity are applied within the hinge. When there is an absence of precise damping control, we assume that the energy loss is through the Rayleigh damping, i.e., they change in proportion to the change of spring stiffness [32,33]. This is reasonable as commonly we place two identical physical torsional springs in parallel to double spring stiffness, and the damping coefficient of this hinge doubles as a result. Based on this assumption, the only independent variables are now the spring stiffness $K = \{k_0, k_1, \ldots, k_{n-1}\}$ at various hinge locations. We aim to acquire appropriate spring stiffness so that no collision amongst panels occurs during deployment. Once a suitable set of stiffness is obtained, corresponding springs can be produced by

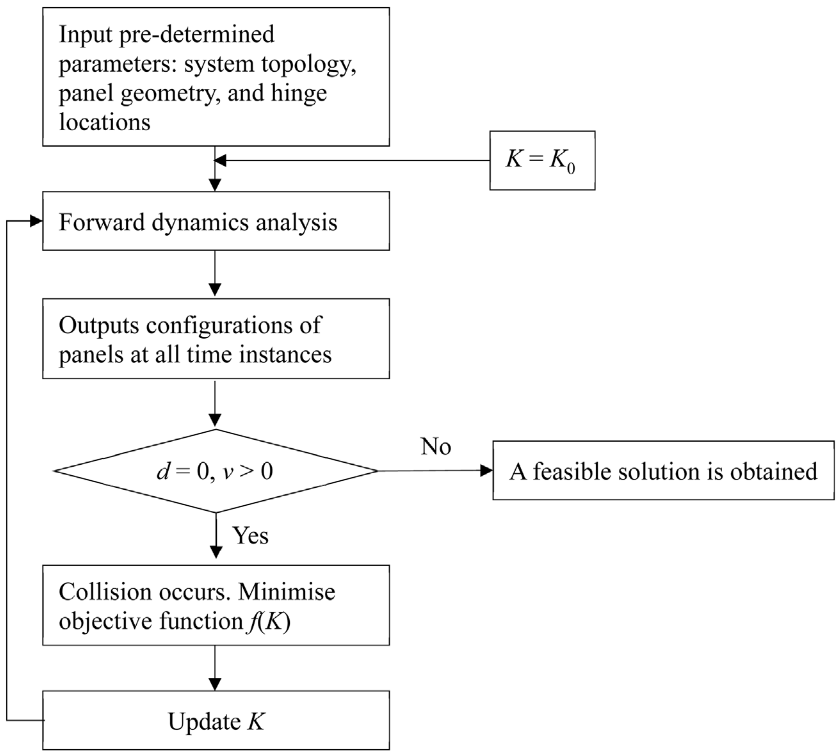

Fig. 4. Flow chart of the optimisation process.

changing their windings during manufacturing. This leads to an optimisation process.

A few parameters need to be introduced first following the collision detection method outlined previously. When collisions are detected at time instance t_J, we calculate vector V_J, defined as the approaching speed of every pair of panels at t_J, using

$$V_J = \frac{D_{J-2} - D_{J-1}}{t_{J-1} - t_{J-2}} \tag{7}$$

and then set the elements in V_J to zero if the corresponding elements in D_J have non-zero values. It is reasonable to assume that $J \geq 3$ since it is less likely in practice that the panels collide after they are just released from stacks. Let d be the smallest element value in D_j and v be the largest element value in V_J. When no collision is detected, V_J is not defined and v is set to zero.

In the optimisation process, we minimise v, the approaching speed if panels collide during the simulation; and maximises d, the minimum proximal distance between any pair of panels if the panels are not in collision. A single-objective function can be formulated as

$$\min f(K) = pv - qd \tag{8}$$

where p and q are pre-set coefficients to make pv and qd unitless. The set of variables to be optimised is $K = \{k_0, k_1, \ldots, k_{n-1}\}$, the stiffness of torsional springs at all hinges. They are allowed to vary within upper and lower bounds specified by the user.

Fig. 4 shows a flow chart of the optimisation process. It starts with an initial set of spring stiffness K_0 as input, which is advanced through dynamic simulation and collision detection. If collisions occur, Matlab function *fmincon* [34] is used to minimise $f(K)$ via an interior-reflective Newton approach [35] aimed to minimise v, the approaching speed between two panels. This leads to a set of updated K. The process is repeated until no collision is detected, indicating that the acquired K is a feasible solution. Among many feasible solutions, it is preferable to have panels as further apart as possible throughout the deployment process. Hence, even after a set of K is obtained with no collisions, we can continue using Matlab function *fmincon* to minimise the objective function $f(K)$ until a local optimum is found. If on the other hand, at the end of the iteration, collisions remain to be unavoidable, for which the objective function is positive, a new set of initial spring stiffness is used to re-run the optimisation process.

4. Physical models and experiments

An array was constructed to demonstrate the effectiveness of the compact packaging scheme and subsequent deployment process without collision. Its topology follows the design in Fig. 2(c), and thus, it contains eight identical smaller panels and four larger panels twice the size of the smaller ones. The geometry of a smaller panel is detailed in the accompanying article in *Data in Brief*. All panels were 3D printed by RAISE 3D N2 using Polylactic acid (PLA) material with 0.15 mm layer resolution and 5% honeycomb infill to obtain a reasonable precision while minimising the mass. With the given hinge arrangement, the array could be folded into two stacks as shown in Fig. 5(b) using the scheme devised with the Hamiltonian circuit.

Two sets of elastic rotational hinges were used to validate its deployment. First, the same torsional springs with stiffness of k_1 =0.1 Nm/rad were used in all rotational hinges, as shown in Fig. 5(a), without implementing any optimisation outlined in this paper. The spring stiffness was tested quasi-statically with a test rig, and the relationship of the moment and rotational angles was plotted in the accompanying article in *Data in Brief*. Two folded stacks of panels were confined by a plastic cable tie and fixed onto the aluminium frame that was mounted on the floor. The deployment process was initiated by cutting the cable tie. A PHOTRON FASTCAM SA-X2 camera recorded the deployment process with a motion capture rate of 1000 fps. The deployment process is presented in Fig. 5(b)–(f) and the accompanying video V1. The large panel in the middle of the array swung back and

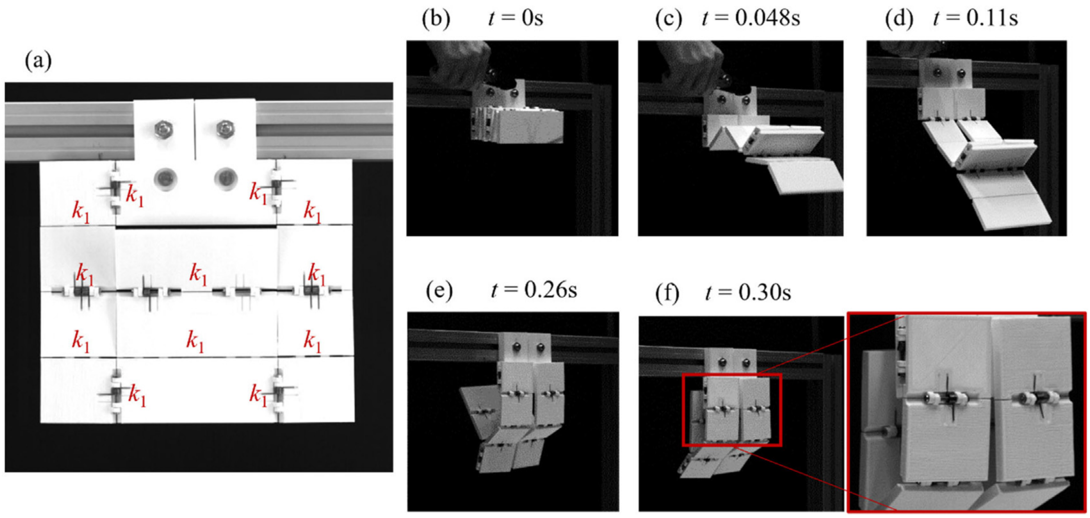

Fig. 5. (a) Torsional springs with the same stiffness $k_1 = 0.1$ Nm/rad were assigned to the hinges. (b)–(f) deployment process of test 1 exhibiting collision at 0.30 s.

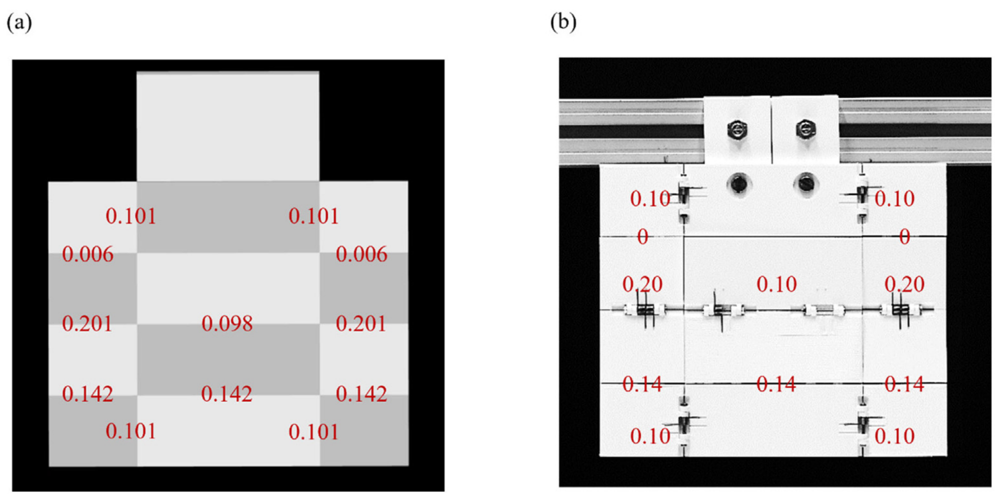

Fig. 6. Spring stiffness assignments at various hinges (in Nm/rad) of (a) the optimised values in the simulation, and (b) the physical model.

collided with the back of the top panel when $t = 0.30$ s, as shown in Fig. 5(f).

To avoid the collision occurring during deployment, an optimisation process was conducted to find a set of suitable spring stiffness. The same spring stiffness was adopted for those springs at symmetrical hinge locations to obtain a symmetrical deployment, with the lower and upper bounds of the stiffness along all hinges to be 0.0010 and 0.2000 Nm/rad, respectively. The optimisation process started with an initial spring stiffness of 0.1000 Nm/rad and a damping coefficient of 0.0043 Nm/(rad/s) at all hinges. The initial damping coefficient for the 0.1000 Nm/rad torsional spring was obtained through performing five free-vibration tests with a set-up shown in Fig. 3 in the accompanying article in *Data in Brief*. A summary of the damping properties was listed in Table 1 of the article, and an average value was taken over five tests. In the optimisation process, the damping coefficient of the spring changes with spring stiffness but remains proportional to it, according to our previous assumptions. The gravitational acceleration g was set to 9.81 m/s^2 in all simulations to model the earth-based deployment processes. Other properties of the hinges that were input to initiate the dynamic simulations were listed in Table 3 of the accompanying article in *Data in Brief*.

A set of optimised spring stiffness was obtained after the optimisation process, which was shown in Fig. 6(a). In the prototype, we conveniently rounded these values up. The stiffness of the hinges used in the prototype was plotted in Fig. 6(b). Since the top two horizontal hinges have rather small stiffness, more than ten times smaller than that of the other springs, we chose to use hinges of zero stiffness for them. Apart from the spring with stiffness 0.10 Nm/rad, another spring with stiffness of 0.07 Nm/rad was also tested quasi-statically using the same test rig, and the result was plotted in Fig. 1(b) of the accompanying article in *Data in Brief*. Some rotational hinges employed two springs placed in parallel to obtain the stiffness shown in Fig. 6(b).

The second set of experiments consisted of a total of five tests. The outcomes were rather consistent, and no collision was observed throughout the deployment processes. Here, we only showed snapshots of the simulated and actual deployment process of one of the tests in Fig. 7 at some characteristic time instances. The complete deployments could be found in the accompanying videos V2 and V3. Overall, the simulated and experimental deployments matched well except at $t = 0.11$ s. The discrepancies might come from the aerodynamic drag in the actual deployment, which was not considered in the simulation, and inaccurate measurement of damping coefficients in the actual prototype.

Since there was no locking mechanism installed at any of the hinges, the panels tended to oscillate around their corresponding equilibrium positions before settling down. This was detected

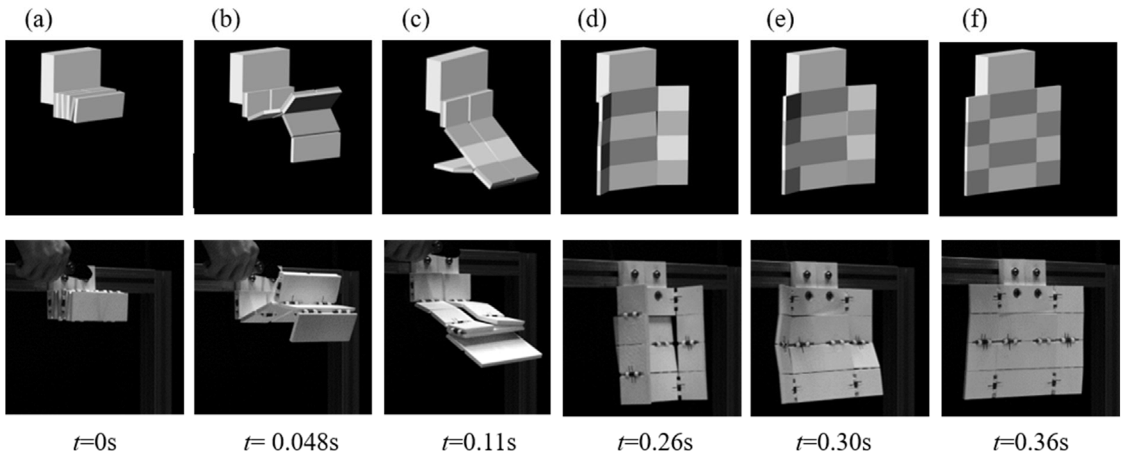

Fig. 7. The simulated (first row) and the actual (second row) deployment process at representative moments.

both in the experiments and simulation though we did not show it here. The deployment was considered to be completed once a flat surface was first reached.

5. Conclusions and discussions

This paper deals with the compact folding of chessboard-like flat arrays into compact bundles and subsequent deployment. On the packaging front, we devised a folding scheme based on the Hamiltonian circuit that can be used successfully to obtain a compact package with two stacks of panels without any voids. The drawback of this approach is that the array processes multiple DoFs, which are inevitable when the number of panels is large, despite that it is possible to reduce the number of DoFs substantially if inactive rotational joints are replaced by rigid joints. This leads us to consider using spring-loaded joints to synchronise the deployment.

We then proposed an effective optimisation method to select the stiffness of rotational joints to ensure a collision-free deployment. Dynamic simulation of deployment and a collision detection method were incorporated into the optimisation process. The sequenced deployment trajectories of panels ensure no collisions occur during deployment, and the array always deploys to a flat surface from packaged stacks.

Both the folding schemes and subsequent deployments were validated successfully by experiments.

It was noticed that the damping coefficient at each hinge is an important parameter that could affect the deployment process. It is, however, rather complex to measure it in the actual prototype, which may explain the small discrepancy between the results of simulation and experiments. This problem can be overcome either by more precise measurement, or incorporating suitable damping control within spring-loaded joints, for instance, by applying packing lubricants with different viscosity within the rotational hinges.

Declaration of competing interest

The authors declare the following financial interests/personal relationships which may be considered as potential competing interests: Jingyi Yang reports financial support was provided by Agency for Science Technology and Research.

Acknowledgements

The authors would like to thank Professor Clive Siviour and his D.Phil student Mr Thomas Commins for borrowing us the PHOTRON high-speed camera and helping us with the settings. We would like to acknowledge Mr Clive Baker for his help manufacturing the test frame for the deployment of the prototypes. In addition, J. Yang would like to thank the Agency for Science, Technology and Research (A*STAR), Singapore, which is financially sponsoring her DPhil studies.

Other data

The data in this manuscript is included in an accompanying article in *Data in Brief*.

References

[1] S.G. Guest, S. Pellegrino, A new concept for solid surface deployable antennas, Acta Astronaut. 38 (2) (1996) 103–113.
[2] F. Santoni, F. Piergentili, S. Donati, M. Perelli, A. Negri, M. Marino, An innovative deployable solar panel system for cubesats, Acta Astronaut. 95 (2014) 210–217.
[3] W. Blackwell, et al., Nanosatellites for earth environmental monitoring: The micromas project, in: 12th Specialist Meeting on Microwave Radiometry and Remote Sensing of the Environment, MicroRad, 2012.
[4] S. Dawson, P. Stella, W. McAlpine, B. Smith, JUNO photovoltaic power at jupiter, in: 10th International Energy Conversion Engineering Conference, Atlanta, Georgia, 2012.
[5] Y. Nishiyama, Miura folding: Applying origami to space exploration, Int. J. Pure Appl. Math. (2012) 269–279.
[6] M. Straubel, M. Hillebrandt, C. Hühne, Evaluation of different architectural concepts for huge deployable solar arrays for electric propelled space crafts, in: 14th European Conference on Spacecraft Structures, Materials and Environmental Testing, Toulouse, France, 2016, pp. 27–30.
[7] S. Guest, S. Pellegrino, Inextensional wrapping of flat membranes, in: Proceedings of the First International Seminar on Structural Morphology, Montpellier, 1992.
[8] S.A. Zirbel, R.J. Lang, M.W. Thomson, D.A. Sigel, P.E. Walkemeyer, B.P. Trease, S.P. Magleby, L.L. Howell, Accommodating thickness in origami-based deployable arrays, J. Mech. Des. (2013).
[9] R. Xu, X. Zhang, J. Ma, Y. Chen, Y. Chao, Z. You, Folding a rigid flat surface around a square hub, in: Proceedings of the ASME 2018 International Design Engineering Technical Conference & Computers and Information in Engineering Conference, IDETC/CIE, Quebec, Canada, 2018.
[10] Y. Chen, R. Peng, Z. You, Origami of thick panels, Science 349 (6246) (2015) 396–400.
[11] B.J. Edmondson, R.J. Lang, M.R. Morgan, S.P. Magleby, L.L. Howell, Thick rigidly foldable structures realized by an offset panel technique, in: Origami 6, Tokyo, Japan, 2015, pp. 149–161.
[12] R.J. Lang, K.A. Tolman, E.B. Crampton, S.P. Magleby, L.L. Howell, A review of thickness-accommodation techniques in origami-inspired engineering, Appl. Mech. Rev (2018).
[13] K.A. Seffen, S. Pellegrino, Deploy. Dynam. Tape Springs 455 (1999) 1003–1048, The Royal Society.
[14] A.M. Watt, S. Pellegrino, Rigid Deployable Solar Array, University of Cambridge, Cambridge, 2004.
[15] F. Santoni, Dynamics of spring-deployed solar panels for agile nanospacecraft, J. Aerosp. Eng. 28 (5) 2015.

[16] W.R. Hamilton, Letter to John T. Graves on the icosian, in: H. Halberstam, R.E. Ingram (Eds.), The Mathematical Papers of Sir William Rowan Hamilton, 17 Oct. 1856, vol. 1931, Cambridge University Press, p. 3, (Algebra).
[17] A. Itai, C.H. Papadimitriou, J.L. Szwarcfiter, Hamilton paths in grid graphs, SIAM J. Comput. 11 (4) (1982) 676–686.
[18] J. Yang, Z. You, Compactly folding rigid panels with uniform thickness through origami and Kirigami, in: ASME IDETC, Anaheim, CA, 2019.
[19] K.H. Hunt, Kinematic Geometry of Mechanisms, Oxford University Press, Oxford, 1978.
[20] C. Fuhrer, B.J. Leimkuhler, Numerical solution of differential–algebraic equations for constrained mechanical motion, Numer. Math. 59 (1991) 55–69.
[21] J. Wang, C.M. Gosselin, L. Cheng, Modeling and simulation of robotic systems with closed kinematic chains using the virtual spring approach, Multibody Syst. Dyn. 7 (2002) 145–170.
[22] M.W. Spong, S. Hutchinson, M. Vidyasagar, Robot Dynamics and Control, Wiley, 2004.
[23] R. Featherstone, Rigid Body Dynamics Algorithms, Springer, Canberra, Austrailia, 2008.
[24] J. Li, S. Yan, F. Guo, P. Guo, Effects of damping, friction, gravity, and flexibility on the dynamic performance of a deployable mechanism with clearance, Proc. Inst. Mech. Eng. C 227 (8) (2013) 1791–1803.
[25] Y. Li, M. Li, Y. Li, X. Ge, C. Cu, Parameter optimization for torsion spring of deployable solar array system with multiple clearance joints considering rigid–flexible coupling dynamics, Chin. J. Aeronaut. (2021).
[26] S. Miller, Simscape multibody multiphysics library, MATLAB central file exchange, 2020, [Online]. Available: https://www.mathworks.com/matlabcentral/fileexchange/37636-simscape-multibody-multiphysics-library. (Accessed 10 January 2020).
[27] Simscape - matlab & simulink, mathworks, R2019b, 2020, [Online]. Available: https://uk.mathworks.com/products/simscape.html. (Accessed 06 March 2020).
[28] P. Bogacki, L.F. Shampine, A 3(2) pair of Runge–Kutta formulas, Appl. Math. Lett. 2 (1989) 321–325.
[29] L.F. Shampine, M.W. Reichelt, The MATLAB ODE suite, SIAM J. Sci. Comput. 18 (1997) 1–22.
[30] E.G. Gilbert, D.W. Johnson, S.S. Keerthi, A fast procedure for computing the distance between complex objects in three-dimensional space, IEEE J. Robot. Autom. 4 (2) (1988).
[31] C. Ericson, Real-Time Collision Detection, CRC Press, 2005.
[32] S. Adhikari, A.S. Phani, Rayleigh's Classical Damping Revisited, 2004, pp. 1–23.
[33] N.I. Gartung, Approaches for the calculation of Rayleigh damping coefficients for a time-history analysis, in: Structures Under Shock and Impact XV, Vol. 180, 2018, pp. 227–237.
[34] Matlab optimization toolbox - fmincon, mathworks, R2019b, 2020, [Online]. Available: https://uk.mathworks.com/help/optim/ug/fmincon.html#References. (Accessed 15 February 2020).
[35] T.F. Coleman, Y. Li, On the convergence of interior-reflective Newton methods for nonlinear minimization subject to bounds, Math. Program. 67 (1994) 189–224.